ACSNANO

www.acsnano.org

ARTICLE

Multiplexed Identification of Bacterial Biofilm Infections Based on Machine-Learning-Aided Lanthanide Encoding

Jie Wang,[‖] Zhuoran Jiang,[‖] Yurong Wei,[‖] Wenjie Wang, Fubing Wang, Yanbing Yang,* Heng Song,* and Quan Yuan*

Cite This: *ACS Nano* 2022, 16, 3300−3310

Read Online

ACCESS | Metrics & More | Article Recommendations | Supporting Information

ABSTRACT: **Pathogenic biofilms are up to 1000-fold more drug-resistant than planktonic pathogens and cause about 80% of all chronic infections worldwide. The lack of prompt and reliable biofilm identification methods seriously prohibits the diagnosis and treatment of biofilm infections. Here, we developed a machine-learning-aided cocktail assay for prompt and reliable biofilm detection. Lanthanide nanoparticles with different emissions, surface charges, and hydrophilicity are formulated into the cocktail kits. The lanthanide nanoparticles in the cocktail kits can offer competitive interactions with the biofilm and further maximize the charge and hydrophilicity differences between biofilms. The physicochemical heterogeneities of biofilms were transformed into luminescence intensity at different wavelengths by the cocktail kits. The luminescence signals were used as learning data to train the random forest algorithm, and the algorithm could identify the unknown biofilms within minutes after training. Electrostatic attractions and hydrophobic−hydrophobic interactions were demonstrated to dominate the binding of the cocktail kits to the biofilms. By rationally designing the charge and hydrophilicity of the cocktail kit, unknown biofilms of pathogenic clinical isolates were identified with an overall accuracy of over 80% based on the random forest algorithm. Moreover, the antibiotic-loaded cocktail nanoprobes efficiently eradicated biofilms since the nanoprobes could penetrate deep into the biofilms. This work can serve as a reliable technique for the diagnosis of biofilm infections and it can also provide instructions for the design of multiplex assays for detecting biochemical compounds beyond biofilms.**

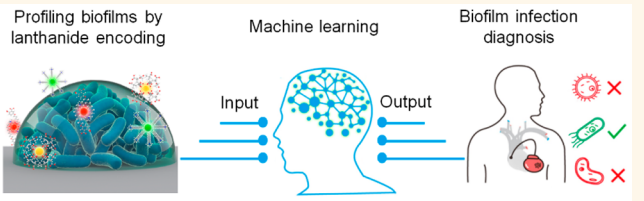

KEYWORDS: *lanthanide, nanoparticles, persistent luminescence, multiplexing, bacteria*

INTRODUCTION

Pathogenic biofilms are responsible for about 65% and 80% of all microbial and chronic infections, respectively, as reported by the National Institutes of Health of America.[1] Biofilm consists of pathogens adhering to the abiotic surface and the self-secreted slimy extra-cellular polysaccharides (EPS) that are tightly wrapped the inner pathogens.[2−4] The EPS protects the pathogens from the attack of an immune defense and antibiotics.[2,5,6] Moreover, the pathogens in biofilms can share drug resistance genes by plasmid exchange.[3,7−9] These features make pathogens in biofilms clinically 1000-fold more resistant to antibiotics compared with planktonic pathogens.[8,10,11,13] To fight biofilm infections, tailor-made therapies are indispensable since the most efficient therapies can only be formulated after doctors ascertain the pathogen species.[12,14,15] However, the complicated biofilm matrix makes biofilm infections clinically challenging in diagnosis.[16] The EPS can prevent the targeting molecules such as antibodies from labeling the inner pathogens because the EPS are difficult to penetrate,[2,17] making the routine antibody-based assay ineffective. PCR-based methods show good reliability in the identification of pathogens.[16] However, the EPS are difficult to lyse, and nucleic acids are vulnerable to fragmentation in the harsh lysate, causing false-positive or false-negative results in biofilm detection by PCR.[16,18] Therefore, developing methods for the prompt and reliable identification of biofilms is crucial for the diagnosis and treatment of biofilm infections.

The EPS mainly consist of polysaccharides, proteins, nucleic acids, and lipids. The chemical composition of the EPS varies among biofilms, suggesting that biofilms display different physicochemical properties such as charge and hydrophilic-

Received: December 20, 2021
Accepted: January 26, 2022
Published: January 31, 2022

https://doi.org/10.1021/acsnano.1c11333
ACS Nano 2022, 16, 3300−3310

Scheme 1. Schematic Diagram of Biofilm Identification with the Machine-Learning-Aided Cocktail Assay[a]

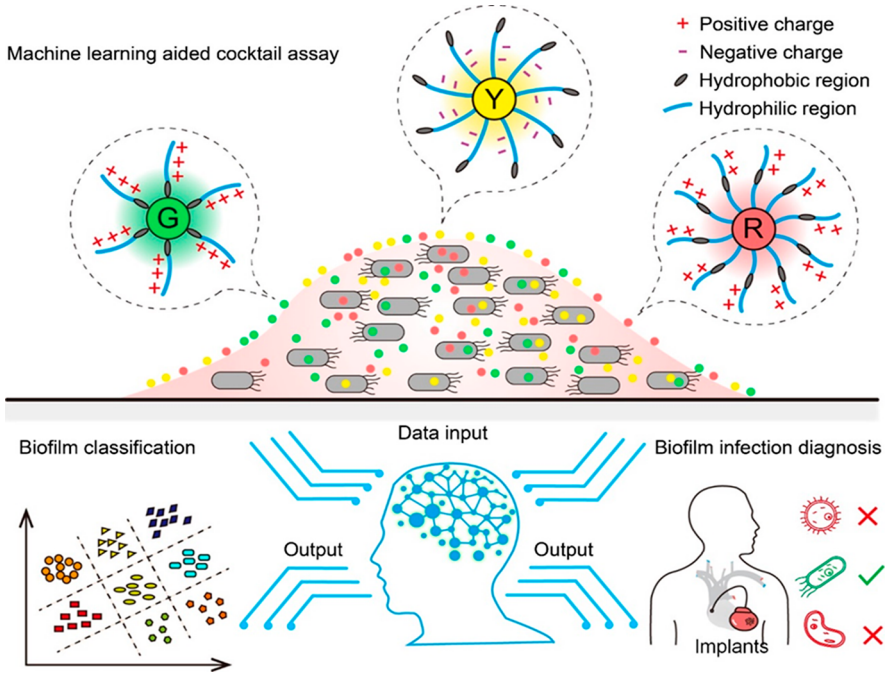

[a]A panel of lanthanide-doped nanoprobes with different emission wavelengths, surface charges, and hydrophilicities are formulated into a cocktail kit. The cocktail kit can bind to the biofilms via interactions that include electrostatic and hydrophobic−hydrophobic interactions. Due to the heterogeneity of biofilms, the lanthanide-doped nanoprobes that accumulate in the biofilms differ from biofilm to biofilm, making it possible to present the characteristic features of biofilms using luminescence signal patterns. The luminescence signals are used as the input data for biofilm classification. Random forest algorithms are trained with the characteristic luminescence signal patterns of biofilms. After training, the random forest algorithms can further identify the unknown biofilms in minutes.

ity.[19,20] Therefore, identifying biofilms by their fingerprint physicochemical properties even without any preknowledge of the specific chemical or biotargets is promising. Reliable biofilm identification can be achieved by defining the signatures of biofilms through multiplexed measurements of the fingerprint physicochemical properties of the EPS. Considering that the physicochemical properties of the EPS might be influenced by the local growth environment,[2] a large number of biofilm samples should be measured to increase the effect sizes and the accuracy of biofilm fingerprint data.[21] Thus, a multiplexed assay with a built-in data processing capability is ideal for prompt and reliable biofilm identification.

Machine learning offers a highly effective tool for parsing massive amounts of data by employing a set of computational algorithms.[22] Herein, we report a machine-learning-aided cocktail assay for biofilm identification by the multiplexed measurement of the fingerprint physicochemical properties. By rationally designing the charge and hydrophilicity of nanoprobes in the cocktail kit, the fingerprint physicochemical properties of biofilms can be obtained for reliable biofilm identification. Electrostatic and hydrophobic−hydrophobic interactions are confirmed to dominate the binding of the nanoprobes to the biofilms. The unknown biofilms of pathogenic clinical isolates and biofilm subtypes were all identified with a random forest algorithm with an overall accuracy of over 80%. Moreover, antibiotic-loaded nanoprobes display an antibacterial efficiency of over 75%, doubling that of single antibiotics. This work establishes a prompt and reliable assay for biofilm identification and treatment and not only can provide instructions for the design of biofilm detection assays but also can be potentially translated into clinical practice for biofilm infection diagnosis and treatment.

RESULTS AND DISCUSSION

The nature of the EPS needs to be taken into consideration in the design of the cocktail kit for discriminating the physicochemical difference between biofilms. Since the EPS of biofilms in nature are efficient in the enrichment of nanoparticles such as sulfide and phosphate,[2] lanthanide-doped luminescence nanoparticles are employed to recognize biofilms. The EPS of biofilms are generally negatively charged,[2] suggesting that positively charged nanoparticles can bind to the EPS easily. However, some molecules in the EPS that are produced by several bacterial species can be positively charged. For instance, polysaccharides are polycationic in *Staphylococcus*.[23] Thus, nanoparticles with negative charges can bind to the positively charged domain of the EPS. Therefore, both positively charged and negatively charged nanoparticles are needed to discriminate the charge difference between biofilms. In EPS, the polysaccharides, proteins, and DNA are amphipathic molecules with both hydrophilic and hydrophobic moieties.[2] These molecules bind to each other via hydrophobic−hydrophobic interaction to form the 3D polymer network of biofilms.[3,24−26] In the hydrated microenvironment, nanoparticles with surface amphipathic ligands can bind to the EPS via hydrophobic−hydrophobic interactions. Thus, nanoparticles with variable hydrophilicity can discriminate the hydrophilicity difference between biofilms. In summary, positively charged and negatively charged lanthanide nanoparticles with variable hydrophilicity are designed for the

https://doi.org/10.1021/acsnano.1c11333
ACS Nano 2022, 16, 3300−3310

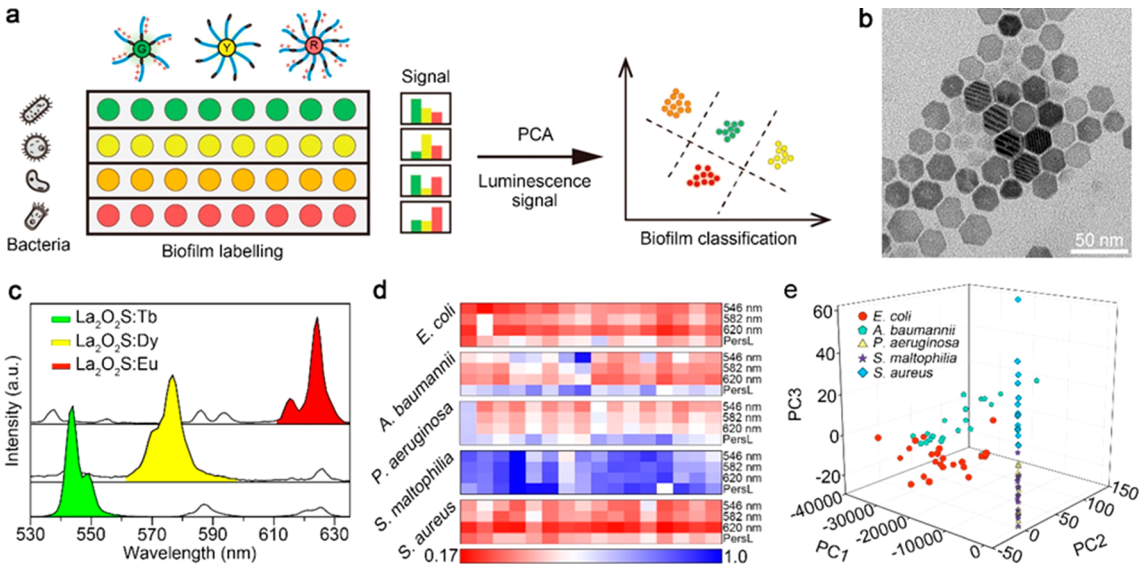

Figure 1. Biofilm classification with the machine-learning-aided cocktail assay. (a) Schematic illustration of labeling and classifying biofilms with the cocktail assay. (b) TEM image of the La_2O_2S:Tb nanoparticles. (c) Photoluminescence spectra of the La_2O_2S:Tb, La_2O_2S:Dy, and La_2O_2S:Eu nanoparticles. (d) Heat map of the normalized photoluminescence luminescence intensity and total PersL intensity from the labeled biofilms (16 samples for each biofilm are shown). (e) Three-dimensional (3D) PCA canonical score plot showing the classification of the biofilms. The amphipathic ligands used are as follows: dextran, cetyltrimethylammonium bromide (CTAB), poly(ether imide) (PEI), 11-(3,4-dicarboxyphenoxy)-*N,N,N*-trimethylundecan-1-aminium chloride (TMA), polyethylene glycol (PEG), and poly(acrylic acid) (PAA). The cocktail kit used is as follows: La_2O_2S:Tb-dextran, La_2O_2S:Dy-CTAB, La_2O_2S:Eu-PEI, Gd_2O_2S:Tb-TMA, Gd_2O_2S:Dy-PEG, and Gd_2O_2S:Eu-PAA.

multiplexed measurement of the physicochemical differences between biofilms.

Scheme 1 summarizes the machine-learning-aided cocktail assay to profile biofilms as a function of their fingerprint physicochemical properties. A panel of lanthanide-doped luminescence nanoparticles with different emissions are employed to construct the multiplexed measurement cocktail kit. Amphipathic ligands with both positive or negative charges and variable hydrophilicity are modified on the surface of the nanoparticles. The presence of these nanoprobes in the cocktail kit can offer competitive interactions with the biofilm and maximize the charge and hydrophilicity differences between biofilms.[21] The fingerprint physicochemical properties of biofilms are transformed into luminescence signals by the cocktail kit. The luminescence signals are fed as learning data to train the random forest algorithm for biofilm classification. After training, the random forest algorithm can identify the unknown biofilms within minutes. In this way, prompt and reliable biofilm identification is realized with the machine-learning-aided cocktail assay.

The lanthanide nanoprobes show the variable binding ability to different biofilms, so the labeled biofilms can produce characteristic luminescence signal patterns for biofilm identification, as illustrated in Figure 1a. The La_2O_2S:Tb/Dy/Eu and Gd_2O_2S:Tb/Dy/Eu nanoparticles[27] are well-dispersed with a diameter of about 25 nm (Figures 1b, S2, and S3). These lanthanide-doped nanoparticles display good crystallinity (Figures S4 and S5) and narrow green, yellow, and red emissions (Figures 1c and S7). Persistent luminescence (PersL) was observed in all of these lanthanide-doped nanoparticles (Figures S8 and S9). The Tb-, Dy-, and Eu-doped nanoparticles were further functionalized by amphipathic ligands with variable charges and hydrophilicities for the preparation of the cocktail kit (Tables S1 and S2 and Figures S13−S18). The prepared lanthanide-doped nanoprobes show good colloidal stability (Figure S19). According to previous studies on in vivo biofilm infections, the following biofilms were selected: *Staphylococcus aureus* (*S. aureus*), *Acinetobacter baumannii* (*A. baumannii*), *Pseudomonas aeruginosa* (*P. aeruginosa*), *Stenotrophomonas maltophilia* (*S. maltophilia*), and *Escherichia coli* (*E. coli*).[14,28,29] *P. aeruginosa*, *S. maltophilia*, and *A. baumannii* were pathogenic clinical isolates provided by the Zhongnan Hospital of Wuhan University.

The designed cocktail kit was further used to classify the above biofilms (Figure S20). Figure 1d summarizes the physicochemical features of the biofilms, presented as the luminescence intensity and the total PersL intensity. Different luminescence signal patterns were observed across the five biofilms, indicating the heterogeneous physicochemical features of different biofilms (Figures 1d and S21). In the preliminary study, principal component analysis (PCA) was employed to classify the biofilms based on the above luminescence data to investigate whether the cocktail kit was promising for biofilm discrimination.[30−32] As shown in Figure 1e, the data groups from the five biofilms show considerable separation in the 3D PCA scatter map, showing that multiplexed measurement of the fingerprint features is promising for biofilm identification. These assays suggest that the cocktail kit can afford variable binding affinities to different biofilms, and the competitive binding of the nanoprobes with the biofilm can maximize the physicochemical differences for efficient biofilm discrimination.

The biofilm discrimination performance of the cocktail assay depends on the interaction between the nanoprobes and the biofilms.[22,30] The interaction forces that govern the binding of the nanoprobes to biofilms were further investigated in an attempt to guide the design of efficacious cocktail kits. La_2O_2S:Tb-based nanoprobes with different surface charges and hydrophilicities were designed as follows: Tb-dextran, Tb-CTAB, Tb-PEI, Tb-TMA, Tb-PEG, Tb-PAA, and Tb-DMPA

https://doi.org/10.1021/acsnano.1c11333
ACS Nano 2022, 16, 3300−3310

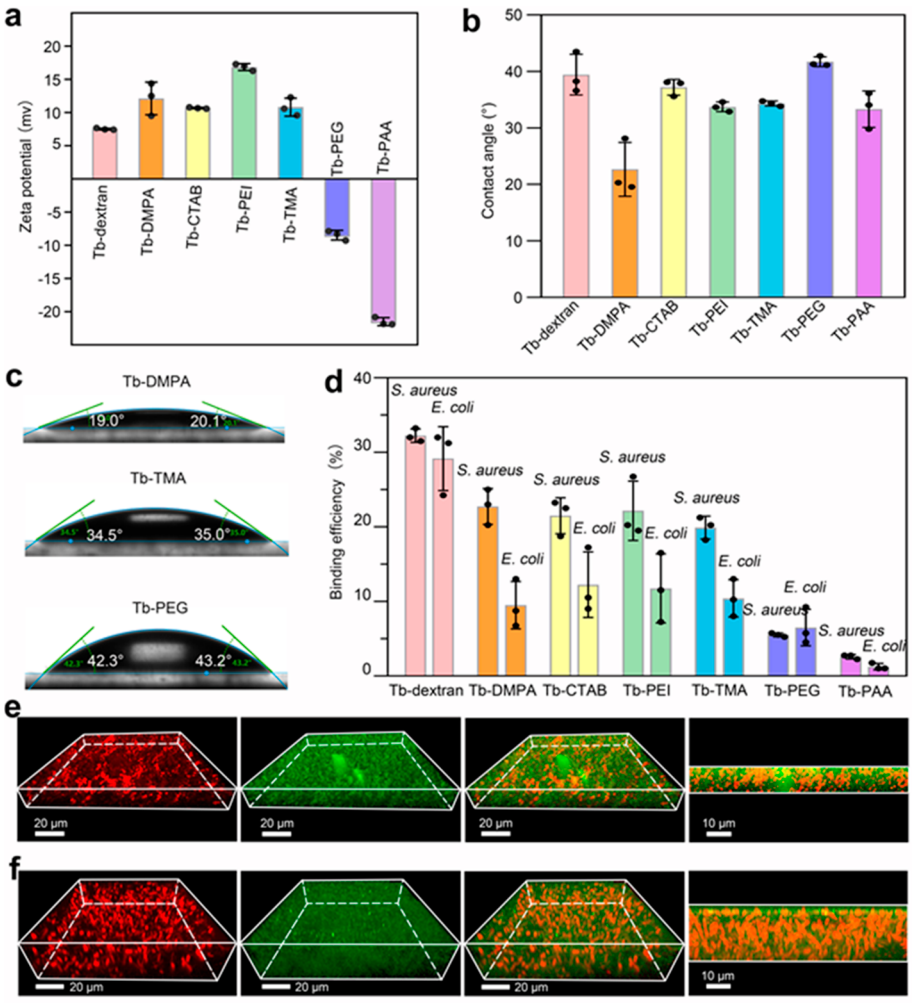

Figure 2. Investigation of the binding of lanthanide-doped nanoprobes to biofilms. (a) ζ-Potentials of the Tb-dextran, Tb-DMPA, Tb-CTAB, Tb-PEI, Tb-TMA, Tb-PEG, and Tb-PAA nanoprobes. (b) Contact angles of the lanthanide nanoprobes with a glass slide. (c) Optical images showing the contact angles of Tb-PEG, Tb-TMA, and Tb-DMPA droplets with a glass slide. (d) The binding efficiencies of the nanoprobes with *S. aureus* and *E. coli* biofilms. Error bars represent the mean ± standard error of the mean (s.e.m.) of three independent experiments. (e and f) 3D surface projection of Z-stack images showing the distributions of the Tb-dextran nanoprobes (green channel) in the *S. aureus* biofilm (red channel) and the *E. coli* biofilm (red channel), respectively.

(Table S1 and S3). The physicochemical properties of these nanoprobes and their binding performance to the biofilms were investigated. Figure 2a shows that the ζ-potential of the nanoprobes ranges from about 17 (Tb-PEI) to −21.5 mV (Tb-PAA), indicating the different surface charges of these nanoprobes. Figure 2b summarizes the contact angle of the lanthanide-doped nanoprobes, showing the different hydrophilicities of these nanoprobes. The contact angle images of the nanoprobe dispersion droplets further show the different hydrophilicities of the nanoprobes (Figures 2c and S23). For easy comparison, the nanoprobes with contact angles below 35° were defined as strongly hydrophilic (Tb-DMPA, Tb-PEI, Tb-TMA, and Tb-PAA), and the other nanoprobes were defined as weakly hydrophilic (Tb-dextran, Tb-CTAB, and Tb-PEG). The binding of these nanoprobes to biofilms was further investigated.

Gram-positive *S. aureus* and Gram-negative *E. coli* were used as the model biofilms. To quantify the binding ability of the lanthanide-doped nanoprobes to *S. aureus* and *E. coli* biofilms, the nanoprobes bound to the biofilms were lysed and further measured by inductively coupled plasma atomic absorption spectrometry. Generally, the positively charged nanoprobes display an enhanced binding ability to both biofilms compared with the negatively charged nanoprobes (Figure 2d). This result confirms that the biofilms are usually negatively charged and the electrostatic attraction between the positively charged nanoprobes and the negatively charged biofilm plays a crucial role in the binding of the nanoprobes to the biofilm. It is worth noting that the binding efficiency of the positively charged nanoprobes to the biofilms does not increase gradually with the increase of the positive charge. Instead, positively charged nanoprobes with weak hydrophilicity (Tb-dextran and Tb-CTAB) display enhanced binding to the biofilms, suggesting that hydrophobic−hydrophobic interactions also contribute to the binding of the lanthanide-doped nanoprobes to the biofilms. The binding of the nanoprobes to the biofilms was further visualized by confocal microscopy. The 3D images show that the *S. aureus* (red channel, Figure 2e) and *E. coli* (red channel, Figure 2f) biofilms are about 7−20 μm thick (Figures S24 and S25). The Tb-dextran nanoprobes (green channel, Figure 2e and f) accumulate on the surface of the *S. aureus* and *E. coli* biofilms. Additionally, the luminescence

https://doi.org/10.1021/acsnano.1c11333
ACS Nano 2022, 16, 3300−3310

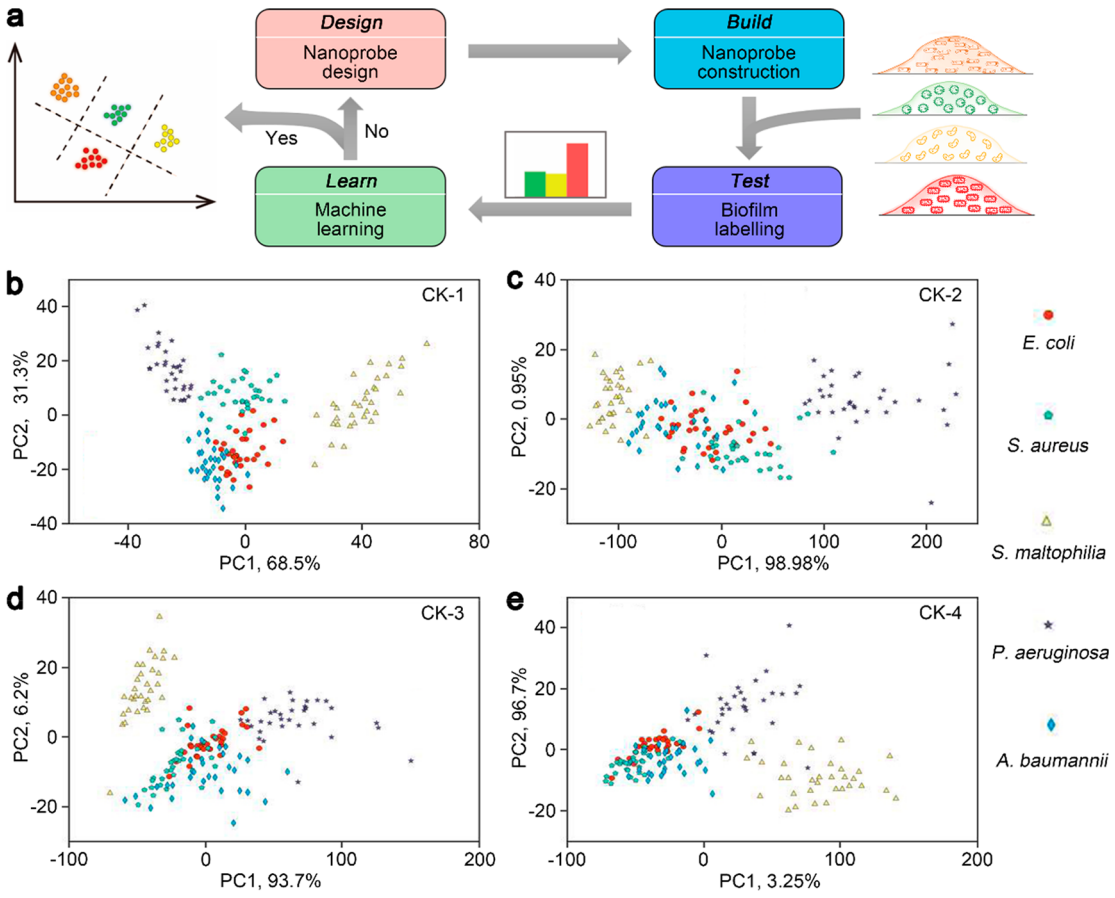

Figure 3. Cocktail kit optimization for efficient biofilm identification. (a) Schematic illustration of the machine-learning-driven DBTL pipeline. (b–e) PCA canonical score plots showing the biofilm discrimination performance of the cocktail kits. CK-1, Tb-PEG/Dy-dextran/Eu-PEI; CK-2, Tb-DMPA/Dy-dextran/Eu-PEG; CK-3, Tb-PAA/Dy-dextran/Eu-PEI; and CK-4, Tb-DMPA/Dy-PEI/Eu-PEG.

signal of the Tb-dextran nanoprobes (green channel) is present in the middle and bottom of the biofilms, suggesting the penetration of the nanoprobes into the EPS of biofilm.[2,19] Other Tb-based nanoprobes show variable penetration depths into the biofilm, suggesting their different binding ability to the biofilms (Figures S24 and S25). The penetration of the nanoprobes into the EPS makes it possible for the nanoprobes to discriminate the composition differences within the EPS between biofilms. The deep penetration of the nanoprobes into biofilms also makes the nanoprobes valuable for delivering antibiotics to the inner bacteria for biofilm ablation. The above assay confirms that both electrostatic attraction and the hydrophobic–hydrophobic interaction play pivotal roles in the binding of the lanthanide nanoprobes to the biofilms.

Having shown the interaction forces that govern the binding of lanthanide-doped nanoprobes to biofilms, a machine-learning-driven design–build–test–learn (DBTL) pipeline was further constructed to optimize the cocktail kit (Figure 3a). To simplify the cocktail kit, three nanoprobes were formulated into a cocktail kit (Table S4). The biofilm classification performance of the cocktail kit was evaluated by machine learning. If the biofilm classification performance is poor, the charge or the hydrophilicity of the nanoprobes in the cocktail kit will be adjusted accordingly, and another DBTL cycle will be initiated. If good biofilm classification performance appears, the cocktail kit will be used for the detection of the unknown biofilm.

To create strong electrostatic attraction and hydrophobic–hydrophobic interactions, we designed the following cocktail kits containing a high portion of positively charged nanoprobes and weak hydrophilic nanoprobes: the Tb-PEG/Dy-dextran/Eu-PEI cocktail kit (named CK-1) and the Tb-DMPA/Dy-dextran/Eu-PEG cocktail kit (named CK-2). In CK-1 and CK-2, two nanoprobes are positively charged and one nanoprobe is negatively charged while two nanoprobes are weakly hydrophilic and one nanoprobe is strongly hydrophilic. The biofilm classification performance of these two cocktail kits is presented in Figure 3b and c. Well-separated scatters of biofilms are visible, confirming that both positively and negatively charged nanoprobes are crucial for maximizing the composition difference between biofilms. The hydrophilicity of the cocktail kit was further increased to check if better biofilm discrimination results could be obtained. The Tb-PAA/Dy-dextran/Eu-PEI cocktail kit (named CK-3) and the Tb-DMPA/Dy-PEI/Eu-PEG cocktail kit (named CK-4) in which only one nanoprobe was weakly hydrophilic were thus designed. These two cocktail kits (CK-3 and CK-4) also displayed good biofilm classification abilities (Figures 3d and e, S26, and S27) but were not better than CK-1. The cocktail kits containing one positively charged nanoprobe and two negatively charged nanoprobes or three positively charged nanoprobes displayed poor biofilm classification performance (Figures S26 and S27). The above results thus suggest that a higher portion of positively charged nanoprobes and weakly hydrophilic nanoprobes in the cocktail kit can differentiate the

https://doi.org/10.1021/acsnano.1c11333
ACS Nano 2022, 16, 3300–3310

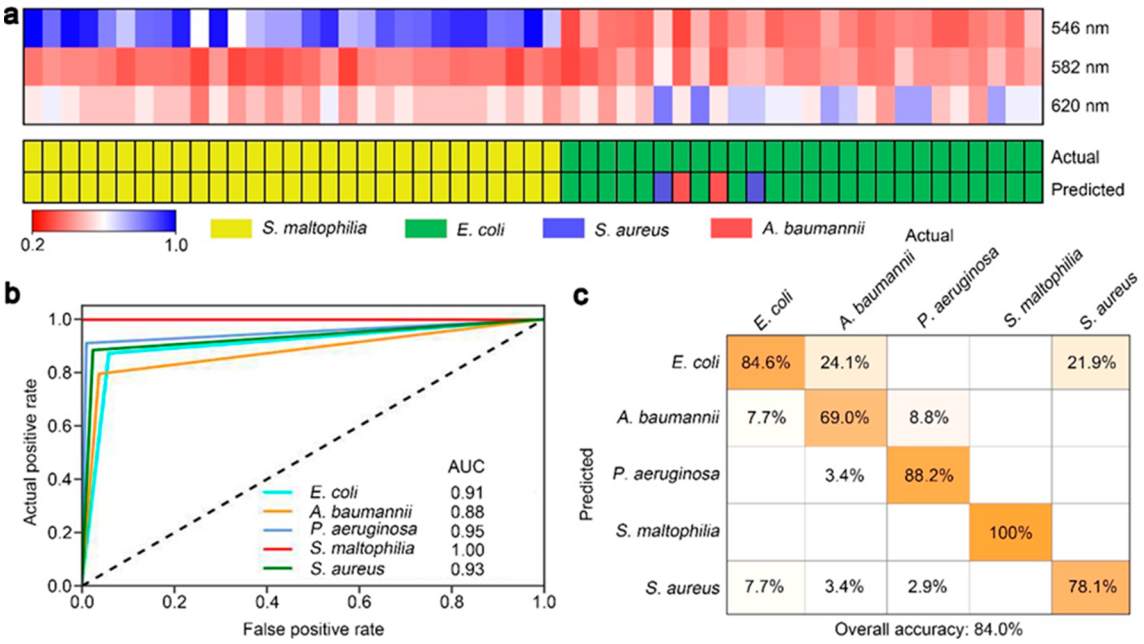

Figure 4. Identification of unknown biofilms with the machine-learning-aided cocktail assay. (a) Application of the trained machine-learning algorithm to an independent validation cohort. The actual and predicted class of the biofilm is shown. (b) ROC curves showing the cocktail assay's success in identifying biofilms. (c) Confusion matrix summarizing the biofilm identification results.

physicochemical heterogeneity between biofilms well. It is noteworthy that the CK-1 cocktail kit displays a better biofilm discrimination performance than the cocktail kit containing six nanoprobes shown in Figure 1e, suggesting that efficient biofilm discrimination can be achieved by the rational design of the cocktail kit.

Having shown the basic principle in the design of the cocktail kit for profiling the biofilm physicochemical heterogeneity, a random forest algorithm was further built for the identification of unknown biofilms. The CK-1 cocktail kit was used here for biofilm labeling. A training cohort containing a total number of 1040 samples of the five biofilms was used to train the algorithm. After training, the unknown biofilm identification performance of the algorithm was tested. The luminescence pattern of the labeled biofilms in the validation cohort and the predicted identity of the biofilm are summarized (Figures 4a and S28). Most of the 150 unknown biofilms were correctly identified by the machine-learning-aided cocktail assay. Particularly, the obtained sensitivity, specificity, and accuracy in identifying *S. maltophilia* are 100%, 100%, and 100%, respectively, suggesting the good reliability of the cocktail assay in biofilm identification (Figures 4a and S28). Receiver operating characteristic (ROC) analysis was utilized to evaluate the identification capability of the machine learning model (Figure 4b). As indicated in Figure 4b, the areas under the ROC curve (AUC) for identifying five kinds of biofilms are all above 0.88, indicating that the cocktail assay exhibits a high accuracy and reliability in biofilm identification. Particularly, the accuracy of the cocktail assay in the identification of the *S. maltophilia* biofilm is 100%. The biofilm identification results were further mapped into a confusion matrix (Figure 4c). The accuracies in identifying *E. coli*, *A. baumannii*, *P. aeruginosa*, *S. maltophilia*, and *S. aureus* are 84.6%, 69.0%, 88.2%, 100%, and 78.1%, respectively. In total, 126 of the 150 unknown biofilm samples were classified correctly, affording an identification accuracy of 84.0%. It is worth mentioning that the whole labeling and identification processes for the given multiple biofilms can be finished in about 1.5 h. These results indicate the feasibility of the cocktail assay in the detection and diagnosis of biofilm infections.

Bacterial drug susceptibility is constantly evolving, and even bacterial strains of the same species show significantly different susceptibilities to antibiotics. The variable drug susceptibility among bacteria subtypes complicates the treatment of infections, especially in the form of biofilm infections.[33−35] The machine-learning-aided cocktail assay was further tested for biofilm subtyping in an attempt to provide potential instruction for clinicians to formulate efficient therapeutic options in the future (Figure 5a). *S. aureus* is among the most frequent bacteria associated with biofilm infections, and several *S. aureus* subtypes with strong drug resistantance have been clinically isolated.[9,28,29] The *S. aureus* subtypes were used to test the biofilm subtyping performance of the machine-learning-aided cocktail assay. The CK-1 cocktail kit was used to label the *S. aureus* subtypes, and the random forest algorithm was trained with the luminescence characteristics of the labeled biofilms. Figure 5b summarizes the luminescence pattern of the labeled *S. aureus* biofilm subtypes in the training cohort, and the different luminescence responses are observed across these biofilms. For instance, the labeled *SA-RN4220* biofilm shows the lowest green emission at 546 nm, whereas the labeled *SA-RN43300* biofilm displays the strongest green and yellow emissions at 546 and 582 nm, respectively, suggesting that the luminescence features could realize efficient *S. aureus* biofilm subtype discrimination. Figure 5c further shows the separation of the data groups from the biofilms, confirming that the cocktail kit is capable of biofilm subtyping. The random forest algorithm was used to learn the luminescence features of the labeled biofilms (360 samples), and the performance of the algorithm in identifying unknown biofilms of *S. aureus* subtypes was investigated. The confusion matrix in Figure 5d shows that the biofilm subtyping accuracy is 90%, clearly demonstrating the robust ability of the cocktail assay in biofilm identification. The above results demonstrated

https://doi.org/10.1021/acsnano.1c11333
ACS Nano 2022, 16, 3300−3310

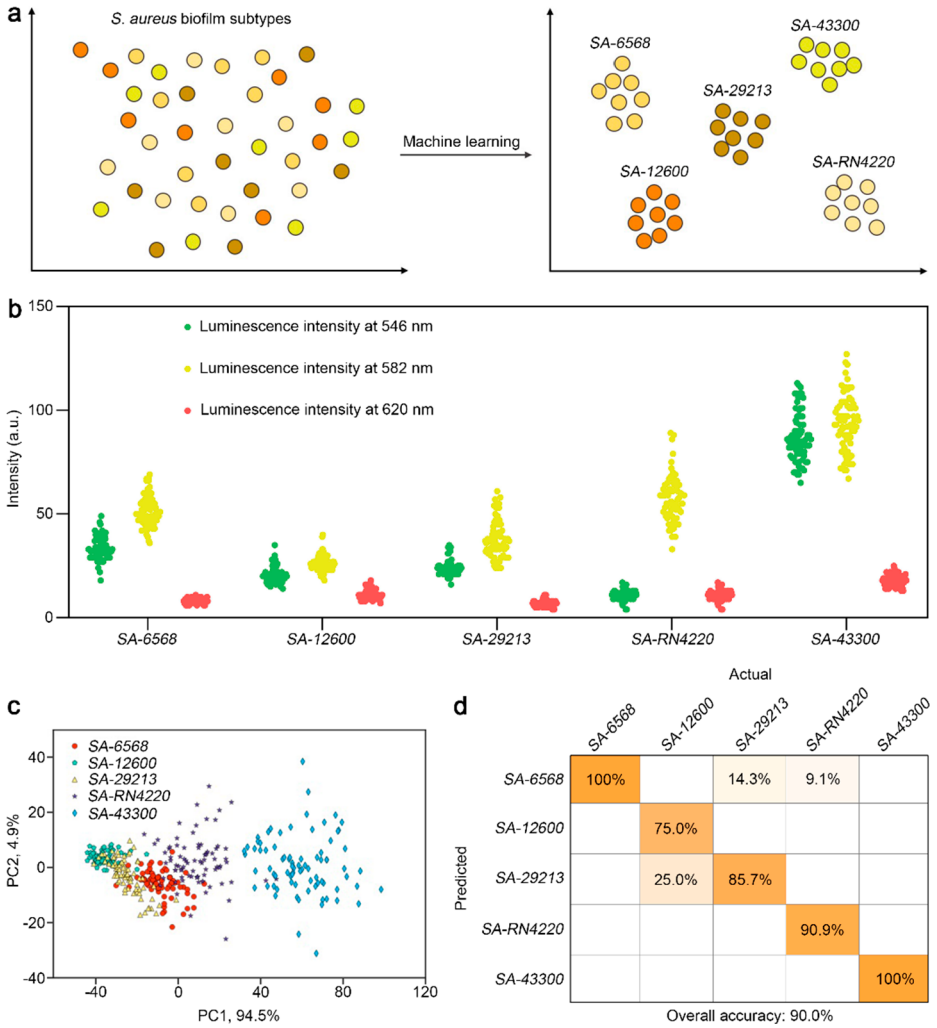

Figure 5. Biofilm subtyping with the machine-learning-aided cocktail assay. (a) Schematic illustration of *S. aureus* biofilm subtyping with the machine-learning-aided cocktail assay. (b) The luminescence intensity pattern of the labeled *S. aureus* biofilm subtypes in the training cohort at different wavelengths. (c) PCA canonical score plots showing the classification of the *S. aureus* biofilm subtypes. (d) Confusion matrix showing the *S. aureus* biofilm subtype identification results in the validation cohort. The sensitivity, specificity, and accuracy in identifying the *SA-6568* biofilm are 100%, 93.8%, and 95.0%, respectively. The sensitivity, specificity, and accuracy in identifying the *SA-12600* biofilm are 75.0%, 100%, and 95.0%, respectively. The sensitivity, specificity, and accuracy in identifying the *SA-29213* biofilm are 85.7%, 94.1%, and 95.0%, respectively. The sensitivity, specificity, and accuracy in identifying the *SA-RN4220* biofilm are 90.9%, 100%, and 97.5%, respectively. The sensitivity, specificity, and accuracy in identifying the *SA-43300* biofilm are 100%, 100%, and 100%, respectively.

the following virtues of the machine-learning-aided cocktail assay: (1) design flexibility, (2) robust discrimination capability, and (3) broad application potentials. The designed machine-learning-aided cocktail assay for biofilm identification and subtyping provides a reliable method for the detection of biocompounds beyond biofilms based on multiplexed recognition assay.[21,36,37]

The potential applications of the cocktail nanoprobes in delivering antibiotics into the EPS for biofilm eradication were further tested. The biofilms treated by Tb-dextran-ampicillin displayed primarily dead cells (red-fluorescent), clearly suggesting that the biofilms were eradicated in large quantities (Figure 6a and b). Tb-dextran-ampicillin affords an antibacterial efficiency of over 75%, doubling that of single ampicillin (Figure 6c and d). These results suggest that the deep penetration of the nanoprobes into biofilms can significantly improve the effectiveness of antibiotics in eradicating biofilms. The performance of Tb-dextran-ampicillin was further tested in eradicating biofilms on pacemakers (Figure S29). With the treatment by bare ampicillin, the *S. aureus* biofilm shows collapsed cells, while the shape of most cells is maintained. In contrast, the cell walls of the *S. aureus* are seriously collapsed in the biofilm treated with Tb-dextran-ampicillin (Figure 6e), confirming the potent ability of Tb-dextran-ampicillin to eradicate biofilms. The similar potent antibacterial performance of Tb-dextran-ampicillin toward the *E. coli* biofilm was also demonstrated (Figure 6f). The above findings demonstrated the promise of the surface-modified lanthanide nanoparticles in biofilm eradication. We have shown that surface modification can affect the binding of lanthanide nanoparticles to biofilms, suggesting that the biofilm eradication performance of the nanoprobes can also be influenced by surface modification. The binding affinity of the nanoparticles to the biofilm and the penetration, accumulation, and distribution of the nanoparticles in biofilms are all influenced by the surface modification.[38] The antibiotic delivery efficiency and the biofilm eradication performance of the lanthanide nanoparticles can be further improved by

https://doi.org/10.1021/acsnano.1c11333
ACS Nano 2022, 16, 3300−3310

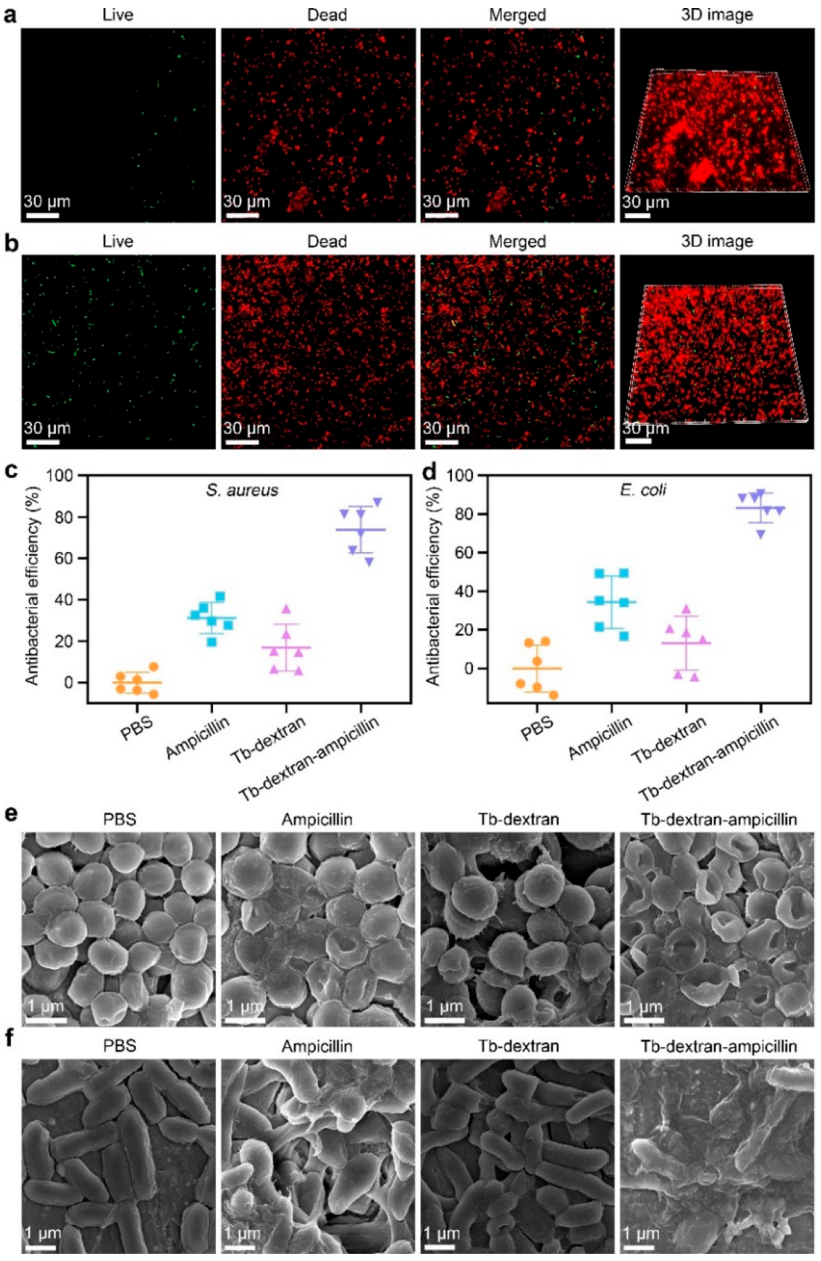

Figure 6. Eradication of biofilms with the lanthanide-doped luminescence nanoprobes. Confocal images of the (a) *S. aureus* (*RN4220*) and (b) *E. coli* biofilms treated by Tb-dextran-ampicillin. The live and dead bacterial cells are indicated by green and red fluorescence, respectively. The 3D surface projection of bacterial cells in the biofilms is shown in the right panel. The antibacterial efficiencies of ampicillin, Tb-dextran, and Tb-dextran-ampicillin toward (c) *S. aureus* (*RN4220*) and (d) *E. coli* biofilms. SEM images showing the (e) *S. aureus* (*RN4220*) and (f) *E. coli* biofilms after different treatments.

optimizing their surface properties. Previous studies demonstrated the great advantages of machine learning in optimizing the surface properties, composition, and structure of nanoparticles in nanomedicines.[39] Thus, the antibacterial performance of the lanthanide nanoprobes can further be optimized in the future by regulating their surface properties with machine learning.[39] The above results thus demonstrate that the cocktail assay can also serve as a practicable strategy for biofilm eradication.

CONCLUSION

In summary, we developed a machine-learning-aided cocktail assay to capture and integrate the fingerprint physicochemical features of biofilms into luminescence signals for prompt and reliable biofilm identification. The cocktail assay displays outstanding performance in identifying unknown biofilms of pathogenic clinical isolates and subtyping biofilms. Importantly, this developed assay not only serves as a reliable technique for the diagnosis of biofilm infections but also provides instructions for the detection of biochemical compounds beyond biofilms. Moreover, the cocktail nanoprobes display high efficiencies in biofilm eradication due to their deep penetration into the biofilms. It is anticipated that the proposed cocktail assay could be readily implemented into the clinical workflow for the reliable diagnosis and efficient treatment of biofilm infections.

https://doi.org/10.1021/acsnano.1c11333
ACS Nano 2022, 16, 3300−3310

EXPERIMENTAL SECTION

Synthesis of the Lanthanide-Doped Ln_2O_2S (La_2O_2S, Gd_2O_2S, and Y_2O_2S) Nanoparticles. The lanthanide-doped Ln_2O_2S nanoparticles were synthesized with a thermal decomposition method.[27] Take the synthesis of La_2O_2S-Tb nanoparticles as an example. Typically, Na(acac) (0.5 mmol), $La(acac)_3$ (0.5 mmol), sulfur powder (0.5 mmol), $Tb(acac)_3$ (0.025 mmol), oleic acid (2.5 mmol), ODE (20 mmol), and oleylamine (17 mmol) were added into a three-neck round-bottom flask (100 mL). The mixture was heated at 120 °C for 30 min under vacuum and vigorous stirring to remove water and other impurities. After that, the resulting solution was heated to 310 °C and was maintained at that temperature for 40 min in Ar gas. The obtained La_2O_2S-Tb nanoparticles were collected by centrifugation after the solution was cooled to room temperature. The La_2O_2S-Tb nanoparticles were further washed with the mixed solution of ethanol and cyclohexane (3:1, v/v) three times. The La_2O_2S-Dy and La_2O_2S-Eu nanoparticles were prepared by the same procedure.

Preparation of PAA-Guided Lanthanide-Doped Ln_2O_2S Nanoprobes. The PAA-guided nanoprobes were prepared according to a previous study.[40] Particularly, 25 mg of the prepared lanthanide-doped Ln_2O_2S nanoparticles were dispersed in 8 mL of chloroform under sonication. Then, the mixture was slowly added into a mixed solution of water (8 mL) and PAA (80 mg). The resultant solution was allowed to react at room temperature for 24 h under vigorous stirring. After that, the aqueous phase was isolated, and the PAA-guided lanthanide-doped Ln_2O_2S nanoprobes were collected by centrifugation (5 min, 6000 rpm).

Preparation of PEI-Guided Lanthanide-Doped Ln_2O_2S Nanoprobes. The PEI-guided nanoprobes were prepared according to a reported method.[41] Briefly, 25 mg of the prepared lanthanide-doped Ln_2O_2S nanoparticles were dispersed in 8 mL of DMSO under sonication. Subsequently, 150 mg of PEI was dissolved in 8 mL of DMSO, and the PEI solution was then added into the dispersion of the above nanoparticles. The resulted mixture solution was refluxed at 95 °C for 5 h under stirring to form a light yellow solution. The PEI-guided Ln_2O_2S nanoprobes were separated by centrifugation.

Preparation of CTAB-Guided Lanthanide-Doped Ln_2O_2S Nanoprobes. First, 25 mg of the prepared lanthanide-doped Ln_2O_2S nanoparticles were added into a mixture solution of cyclohexane (4 mL) and chloroform (4 mL) under sonication. Subsequently, 50 mg of CTAB in 8 mL of deionized water was added into the above solution. The mixed solution was then heated at 40 °C for 24 h under vigorous stirring. The resultant CTAB-guided lanthanide-doped Ln_2O_2S nanoprobes were centrifuged and washed with water three times.

Preparation of TMA- or DMPA-Guided Lanthanide-Doped Ln_2O_2S Nanoprobes. In brief, 25 mg of the prepared lanthanide-doped Ln_2O_2S nanoparticles were dispersed in 8 mL of the mixed solution of cyclohexane and chloroform (1:1, v/v). Then, 50 mg of TMA was dissolved into 8 mL of water by adjusting the pH of the solution to 10 with NaOH. The TMA solution was added to the above dispersion of Ln_2O_2S nanoparticles, and the mixture was stirred for 24 h at 40 °C. The TMA-guided lanthanide-doped Ln_2O_2S nanoprobes were collected by centrifugation and washed. The DMPA-guided lanthanide-doped Ln_2O_2S nanoprobes were prepared with the same protocol.

Preparation of PEG-Guided Lanthanide-Doped Ln_2O_2S Nanoprobes. The PEG-guided nanoprobes were also prepared with a reported method.[42] Briefly, 25 mg of the prepared lanthanide-doped Ln_2O_2S nanoparticles and 2.5 mg of PEG were dispersed in 8 mL of acetone by sonication. Then, 8 mL of Twain-80 was dropwise added into the above dispersion of Ln_2O_2S nanoparticles under vigorous stirring. The mixed solution was allowed to react for 24 h at room temperature. The PEG-guided lanthanide-doped Ln_2O_2S nanoprobes were collected by centrifugation and washing.

Preparation of Dextran-Guided Lanthanide-Doped Ln_2O_2S Nanoprobes. A previously reported protocol was used to prepare the dextran-guided nanoprobes.[43] The prepared lanthanide-doped Ln_2O_2S nanoparticles (50 mg) were dispersed in an aqueous solution (7 mL) containing 500 mg of dextran. The mixture solution was sonicated for 10 min and then further allowed to react at room temperature for 12 h under vigorous stirring. Finally, the dextran-guided lanthanide-doped Ln_2O_2S nanoprobes were collected by centrifugation and washed with distilled water three times.

Biofilm Culture in a 96-Well Microplate. The *E. coli* DH5α strain was streaked onto Lysogeny broth (LB) agar plates, and the plates were incubated at 30 °C overnight. A single colony of *E. coli* DH5α was taken and cultured in 10 mL of LB medium (10 g of Bacto-tryptone, 5 g of yeast extract, and 10 g of NaCl per liter of water) at 37 °C with constant shaking (225 rpm) for 8 h. The bacteria were collected by centrifugation and washed with PBS (10 mM, pH 7.4) three times, followed by redispersion in a modified LB medium (0.1% glucose,1 mM $MgSO_4$, 0.15 M ammonium sulfate, and 34 mM citrate buffered to pH 7). For biofilm formation, the *E. coli* DH5α strains were routinely grown in the modified LB medium to ensure bacterial adherence to the base. The concentration of the bacteria was determined by measuring the OD_{600} value. Seeding solutions were prepared by diluting the bacteria solution with LB medium until the OD_{600} value reached about 0.1. Then, 200 μL aliquots of the seeding solutions were added to each well, and the plates were incubated at 16 °C for three days under static conditions. Fresh modified LB medium was added on day 2. Thereafter, the specimens were carefully rinsed twice with PBS to remove planktonic bacteria. The *S. aureus*,[44] *P. aeruginosa*, *A. baumannii*, and *S. maltophilia* biofilms were prepared with the same procedure.

Biofilm Labeling with the Cocktail Kits. For cocktail kits containing all positively charged nanoprobes, the nanoprobes were mixed directly to prepare the cocktail kits for biofilm labeling. For instance, Tb-PAA (140 mg/L), Dy-dextran (140 mg/L), and Eu-PEI (140 mg/L) were directly mixed to prepare a cocktail kit. Typically, 200 μL of the cocktail kit solution was added into each biofilm-colonized well, and the 96-well microplate was further incubated at 25 °C for 30 min. After incubation, the suspension was gently removed, and the biofilm in each well was washed three times with PBS. For biofilm labeling with cocktail kits containing both positively charged and negatively charged nanoprobes, the biofilm was first labeled with the positively charged nanoprobes, followed by the negatively charged ones. For instance, in biofilm labeling with the CK-4 (Tb-PEG/Dy-dextran/Eu-PEI) kit, the biofilms were first treated with the mixture of Dy-dextran (140 mg/L) and Eu-PEI (140 mg/L) for 30 min at 25 °C, followed by washing with PBS. Then, the biofilms were further incubated with Tb-PEG (140 mg/L) for 30 min and washed with PBS. The luminescence intensities from the labeled biofilms at 546, 582, and 620 nm were recorded on a Tecan 2000 Enzyme microplate reader (Infinite M200 PRO). The total PersL intensity from the labeled biofilms was measured on an IVIS Lumina XR Imaging System using a portable UV lamp as the excitation source.

Machine-Learning Algorithm. The machine-learning model was built based on a random forest algorithm for multiclass classification with 75% of data collected for the training set and 25% collected for the testing set. The computation work was performed using Jupyter Notebook with Python scripts.

Visualizing the Antibacterial Performance of Tb-Dextran-Ampicillin. For confocal observation, biofilms cultured in the confocal dishes were treated with Tb-dextran-ampicillin (140 mg/L). After washing, the biofilms were stained by green-fluorescent Calcein-AM and red-fluorescent propidium iodide for confocal microscopy observation. For the SEM observation, biofilms attached to the pacemakers were treated with ampicillin (0.1 mg/mL), Tb-dextran (140 mg/L), or Tb-dextran-ampicillin in LB (140 mg/L). The treated biofilms were fixed overnight with 2.5% glutaraldehyde. The biofilms samples were dehydrated with sequential ethanol treatments and further observed by a scanning electron microscope.

Quantifying the Antibacterial Ability of Tb-Dextran-Ampicillin Nanoprobes. The colorimetric 3-(4,5-dimethylthiazol-2-yl)-2,5-diphenyl tetrazolium bromide (MTT) assay was employed to quantify the antimicrobial performance of Tb-dextran-ampicillin.[45] The biofilms were formed in 96-well plates. Then, 100 μL of fresh LB medium, ampicillin in LB (0.1 mg/mL), or Tb-dextran-ampicillin in LB (140 mg/L) was added into the wells. The amount of ampicillin in

https://doi.org/10.1021/acsnano.1c11333
ACS Nano 2022, 16, 3300−3310

the Tb-dextran-ampicillin solution (100 μL) is 0.01 mg. After incubation at 37 °C for 24 h, the biofilms were gently washed with sterile normal saline. Each well was pipetted with 90 μL of sterile normal saline and 10 μL of the MTT solution (5.0 mg/mL). The plate was further incubated at 37 °C for 3 h. The insoluble substance in the wells was then dissolved using 100 μL of dimethyl sulfoxide. The absorbance of the obtained solution at 595 nm was recorded on a microplate reader.

ASSOCIATED CONTENT

Supporting Information

The Supporting Information is available free of charge at https://pubs.acs.org/doi/10.1021/acsnano.1c11333.

The synthesis protocol for the organic ligands, the composition of the cocktail kits, TEM images of the nanoparticles, XRD and EDS analysis of the nanoparticles, NMR and MS spectra of the organic ligands, contact angle images, 3D luminescence images of the labeled biofilms, the luminescence pattern of biofilms labeled by different cocktail kits, the biofilm classification performance of different cocktail kits, the actual and predicted identity of biofilms, and images of the pacemaker and the attached biofilms (PDF)

AUTHOR INFORMATION

Corresponding Authors

Quan Yuan − *Key Laboratory of Biomedical Polymers of Ministry of Education, College of Chemistry and Molecular Sciences, School of Microelectronics, Wuhan University, Wuhan 430072, China; Institute of Chemical Biology and Nanomedicine, Molecular Science and Biomedicine Laboratory (MBL), State Key Laboratory of Chemo/Biosensing and Chemometrics, College of Chemistry and Chemical Engineering, Hunan University, Changsha 410082, China*; orcid.org/0000-0002-3085-431X; Email: yuanquan@whu.edu.cn

Heng Song − *Key Laboratory of Biomedical Polymers of Ministry of Education, College of Chemistry and Molecular Sciences, School of Microelectronics, Wuhan University, Wuhan 430072, China*; orcid.org/0000-0002-0049-5053; Email: hengsong@whu.edu.cn

Yanbing Yang − *Key Laboratory of Biomedical Polymers of Ministry of Education, College of Chemistry and Molecular Sciences, School of Microelectronics, Wuhan University, Wuhan 430072, China*; Email: yangyanbing@whu.edu.cn

Authors

Jie Wang − *Key Laboratory of Biomedical Polymers of Ministry of Education, College of Chemistry and Molecular Sciences, School of Microelectronics, Wuhan University, Wuhan 430072, China*

Zhuoran Jiang − *Key Laboratory of Biomedical Polymers of Ministry of Education, College of Chemistry and Molecular Sciences, School of Microelectronics, Wuhan University, Wuhan 430072, China*

Yurong Wei − *Key Laboratory of Biomedical Polymers of Ministry of Education, College of Chemistry and Molecular Sciences, School of Microelectronics, Wuhan University, Wuhan 430072, China*

Wenjie Wang − *Institute of Chemical Biology and Nanomedicine, Molecular Science and Biomedicine Laboratory (MBL), State Key Laboratory of Chemo/Biosensing and Chemometrics, College of Chemistry and Chemical Engineering, Hunan University, Changsha 410082, China*

Fubing Wang − *Department of Laboratory Medicine and Center for Gene Diagnosis, Zhongnan Hospital of Wuhan University, Wuhan University, Wuhan 430062, China*; orcid.org/0000-0002-5971-2622

Complete contact information is available at: https://pubs.acs.org/10.1021/acsnano.1c11333

Author Contributions

[‖]These authors contributed equally to this work. Q.Y., H.S., and Y.Y. designed the project. J.W. and Y.W. synthesized the luminescence nanoparticles. Z.J. and Y.W. performed the biofilm labeling experiments. H.S. performed machine learning analysis. F.W. provided the *P. aeruginosa*, *A. baumannii*, and *S. maltophilia* clinical isolates. J.W. and Y.W. performed the biofilm eradication experiments. W.W. drew the schematic illustration. Z.J. and Y.W. were primarily responsible for data collection. J.W., Q.Y. H.S., and Y.Y. analyzed the results and prepared the manuscript and figures. All authors contributed to the discussion and editing of the manuscript.

Funding

This work was supported by the National Natural Science Foundation of China (21925401, 21904100, and 21904033) and the National Key R&D Program of China (2017YFA0208000 and 2019YFA0210500).

Notes

The authors declare no competing financial interest.

ACKNOWLEDGMENTS

The authors wish to acknowledge the large-scale instrument and equipment sharing the foundation of Wuhan University.

REFERENCES

(1) Jamal, M.; Ahmad, W.; Andleeb, S.; Jalil, F.; Imran, M.; Nawaz, M. A.; Hussain, T.; Ali, M.; Rafiq, M.; Kamil, M. A. Bacterial Biofilm and Associated Infections. *J. Chin. Med. Assoc.* **2018**, *81*, 7−11.

(2) Flemming, H.; Wingender, J. The Biofilm Matrix. *Nat. Rev. Microbiol.* **2010**, *8*, 623−633.

(3) Teschler, J. K.; Zamorano-Sánchez, D.; Utada, A. S.; Warner, C. J. A.; Wong, G. C. L.; Linington, R. G.; Yildiz, F. H. Living in the Matrix: Assembly and Control of *Vibrio cholerae* Biofilms. *Nat. Rev. Microbiol.* **2015**, *13*, 255−268.

(4) Zhang, P.; Chen, Y.; Qiu, J.; Dai, Y.; Feng, B. Imaging the Microprocesses in Biofilm Matrices. *Trends Biotechnol.* **2019**, *37*, 214−226.

(5) He, L.; Le, K. Y.; Khan, B. A.; Nguyen, T. H.; Hunt, R. L.; Bae, J. S.; Kabat, J.; Zheng, Y.; Cheung, G. Y. C.; Li, M.; Otto, M. Resistance to Leukocytes Ties Benefits of Quorum Sensing Dysfunctionality to Biofilm Infection. *Nat. Microbiol.* **2019**, *4*, 1114−1119.

(6) Koo, H.; Allan, R. N.; Howlin, R. P.; Stoodley, P.; Hallstoodley, L. Targeting Microbial Biofilms: Current and Prospective Therapeutic Strategies. *Nat. Rev. Microbiol.* **2017**, *15*, 740−755.

(7) Whiteley, M.; Diggle, S. P.; Greenberg, E. P. Progress in and Promise of Bacterial Quorum Sensing Research. *Nature* **2017**, *551*, 313−320.

(8) Mah, T.; O'Toole, G. A. Mechanisms of Biofilm Resistance to Antimicrobial Agents. *Trends Microbiol.* **2001**, *9*, 34−39.

(9) Arciola, C. R.; Campoccia, D.; Speziale, P.; Montanaro, L.; Costerton, J. W. Biofilm Formation in *Staphylococcus* Implant Infections. A Review of Molecular Mechanisms and Implications for Biofilm-Resistant Materials. *Biomaterials* **2012**, *33*, 5967−5982.

(10) Dieltjens, L.; Appermans, K.; Lissens, M.; Lories, B.; Kim, W.; Van der Eycken, E. V.; Foster, K. R.; Steenackers, P. H. Inhibiting

Bacterial Cooperation is an Evolutionarily Robust Anti-Biofilm Strategy. *Nat. Commun.* **2020**, *11*, 107.
(11) Hallstoodley, L.; Costerton, J. W.; Stoodley, P. Bacterial Biofilms: From the Natural Environment to Infectious Diseases. *Nat. Rev. Microbiol.* **2004**, *2*, 95−108.
(12) Fisher, R. A.; Gollan, B.; Helaine, S. Persistent Bacterial Infections and Persister Cells. *Nat. Rev. Microbiol.* **2017**, *15*, 453−464.
(13) Kim, J. Y.; Sahu, S.; Yau, Y. H.; Wang, X.; Shochat, S. G.; Nielsen, P. H.; Dueholm, M. S.; Otzen, D. E.; Lee, J.; Delos Santos, M. M.; Yam, J. K. H.; Kang, N. Y.; Park, S. J.; Kwon, H.; Seviour, T.; Yang, L.; Givskov, M.; Chang, Y. J. Detection of Pathogenic Biofilms with Bacterial Amyloid Targeting Fluorescent Probe, CDy11. *J. Am. Chem. Soc.* **2016**, *138*, 402−407.
(14) Haunreiter, V. D.; Boumasmoud, M.; Häffner, N.; Wipfli, D.; Leimer, N.; Rachmühl, C.; Kühnert, D.; Achermann, Y.; Zbinden, R.; Benussi, S.; Vulin, C.; Zinkernagel, S. A. In-Host Evolution of *Staphylococcus epidermidis* in a Pacemaker-Associated Endocarditis Resulting in Increased Antibiotic Tolerance. *Nat. Commun.* **2019**, *10*, 1149.
(15) Li, S.; Leung, P.; Xu, X.; Wu, C. Homogentisic Acid γ-Lactone Suppresses the Virulence Factors of *Pseudomonas aeruginosa* by Quenching its Quorum Sensing Signal Molecules. *Chin. Chem. Lett.* **2018**, *29*, 313−316.
(16) Tan, S. Y.; Chew, S. C.; Tan, S. Y.; Givskov, M.; Yang, L. Emerging Frontiers in Detection and Control of Bacterial Biofilms. *Curr. Opin. Biotechnol.* **2014**, *26*, 1−6.
(17) Landis, R. F.; Li, C.; Gupta, A.; Lee, Y.; Yazdani, M.; Ngernyuang, N.; Altinbasak, I.; Mansoor, S.; Khichi, M. A. S.; Sanyal, A.; Rotello, V. M. Biodegradable Nanocomposite Antimicrobials for the Eradication of Multidrug-Resistant Bacterial Biofilms without Accumulated Resistance. *J. Am. Chem. Soc.* **2018**, *140*, 6176−6182.
(18) Costerton, J. W.; Post, J. C.; Ehrlich, G. D.; Hu, F. Z.; Kreft, R.; Nistico, L.; Kathju, S.; Stoodley, P.; Hall-Stoodley, L.; Maale, G.; James, G.; Sotereanos, N.; DeMeo, P. New Methods for the Detection of Orthopedic and Other Biofilm Infections. *FEMS Immunol. Med. Microbiol.* **2011**, *61*, 133−140.
(19) Makabenta, J. M. V.; Nabawy, A.; Li, C.-H.; Schmidt-Malan, S.; Patel, R.; Rotello, V. M. Nanomaterial-Based Therapeutics for Antibiotic-Resistant Bacterial Infections. *Nat. Rev. Microbiol.* **2021**, *19*, 23−36.
(20) Joseph, R.; Naugolny, A.; Feldman, M.; Herzog, I. M.; Fridman, M.; Cohen, Y. Cationic Pillararenes Potently Inhibit Biofilm Formation without Affecting Bacterial Growth and Viability. *J. Am. Chem. Soc.* **2016**, *138*, 754−757.
(21) Diehl, K. L.; Anslyn, E. V. Array Sensing Using Optical Methods for Detection of Chemical and Biological Hazards. *Chem. Soc. Rev.* **2013**, *42*, 8596−8611.
(22) Ko, J.; Baldassano, S. N.; Loh, P. L.; Kording, K.; Litt, B.; Issadore, D. Machine Learning to Detect Signatures of Disease in Liquid Biopsies−a User's Guide. *Lab Chip* **2018**, *18*, 395−405.
(23) Götz, F. *Staphylococcus* and Biofilms. *Mol. Microbiol.* **2002**, *43*, 1367−1378.
(24) Passos da Silva, D.; Matwichuk, M. L.; Townsend, D. O.; Reichhardt, C.; Lamba, D.; Wozniak, D. J.; Parsek, M. R. The *Pseudomonas aeruginosa* Lectin LecB Binds to the Exopolysaccharide Psl and Stabilizes the Biofilm Matrix. *Nat. Commun.* **2019**, *10*, 2183.
(25) Renner, L. D.; Weibel, D. B. Physicochemical Regulation of Biofilm Formation. *MRS Bull.* **2011**, *36*, 347−355.
(26) Van Wolferen, M.; Orell, A.; Albers, S. V. S. Archaeal Biofilm Formation. *Nat. Rev. Microbiol.* **2018**, *16*, 699−713.
(27) Ding, Y.; Gu, J.; Ke, J.; Zhang, Y. W.; Yan, C. H. Sodium Doping Controlled Synthesis of Monodisperse Lanthanide Oxysulfide Ultrathin Nanoplates Guided by Density Functional Calculations. *Angew. Chem., Int. Ed.* **2011**, *50*, 12330−12334.
(28) Sohail, M. R.; Uslan, D. Z.; Khan, A. H.; Friedman, P. A.; Hayes, D. L.; Wilson, W. R.; Steckelberg, J. M.; Stoner, S.; Baddour, L. M. Management and Outcome of Permanent Pacemaker and Implantable Cardioverter-Defibrillator Infections. *J. Am. Coll. Cardiol.* **2007**, *49*, 1851−1859.
(29) Vergidis, P.; Patel, R. Novel Approaches to the Diagnosis, Prevention, and Treatment of Medical Device-Associated Infections. *Infect. Dis. Clin. N. Am.* **2012**, *26*, 173−186.
(30) Yu, K.; Beam, A. L.; Kohane, I. S. Artificial Intelligence in Healthcare. *Nat. Biomed. Eng.* **2018**, *2*, 719−731.
(31) Liu, C.; Zhao, J.; Tian, F.; Cai, L.; Zhang, W.; Feng, Q.; Chang, J.; Wan, F.; Yang, Y.; Dai, B.; Cong, Y.; Ding, B.; Sun, J. S.; Tan, W. H. Low-Cost Thermophoretic Profiling of Extracellular-Vesicle Surface Proteins for the Early Detection and Classification of Cancers. *Nat. Biomed. Eng.* **2019**, *3*, 183−193.
(32) Li, B.; Li, X.; Dong, Y.; Wang, B.; Li, D. Y.; Shi, Y. M.; Wu, Y. Y. Colorimetric Sensor Array Based on Gold Nanoparticles with Diverse Surface Charges for Microorganisms Identification. *Anal. Chem.* **2017**, *89*, 10639−10643.
(33) Jadhav, S.; Bhave, M.; Palombo, E. A. Methods Used for the Detection and Subtyping of *Listeria monocytogenes*. *J. Microbiol. Methods* **2012**, *88*, 327−341.
(34) Antonoplis, A.; Zang, X. Y.; Huttner, M. A.; Chong, K. K. L.; Lee, Y. B.; Co, J. Y.; Amieva, M. R.; Kline, K. A.; Wender, P. A.; Cegelski, L. A Dual-Function Antibiotic-Transporter Conjugate Exhibits Superior Activity in Sterilizing MRSA Biofilms and Killing Persister Cells. *J. Am. Chem. Soc.* **2018**, *140*, 16140−16151.
(35) Siemon, T.; Steinhauer, S.; Christmann, M. Synthesis of (+)-Darwinolide, a Biofilm-Penetrating Anti-MRSA Agent. *Angew. Chem., Int. Ed.* **2019**, *58*, 1120−1122.
(36) Fan, Y.; Wang, S.; Zhang, F. Optical Multiplexed Bioassays Improve Biomedical Diagnostics. *Angew. Chem., Int. Ed.* **2019**, *58*, 13208−13219.
(37) Heinzmann, K.; Carter, L. M.; Lewis, J. S.; Aboagye, E. O. Multiplexed Imaging for Diagnosis and Therapy. *Nat. Biomed. Eng.* **2017**, *1*, 697−713.
(38) Tang, G. H.; He, J. Y.; Liu, J. W.; Yan, X. Y.; Fan, K. L. Nanozyme for Tumor Therapy: Surface Modification Matters. *Exploration* **2021**, *1*, 75−89.
(39) Ho, D.; Wang, P.; Kee, T. Artificial Intelligence in Nanomedicine. *Nanoscale Horiz.* **2019**, *4*, 365−377.
(40) Li, Z.; Lv, S.; Wang, Y.; Chen, S.; Liu, Z. Construction of LRET-Based Nanoprobe Using Upconversion Nanoparticles with Confined Emitters and Bared Surface as Luminophore. *J. Am. Chem. Soc.* **2015**, *137*, 3421−3427.
(41) Tan, Y.; Hu, X. X.; Liu, M.; Liu, X. W.; Lv, X. B.; Li, Z. H.; Wang, J.; Yuan, Q. Simultaneous Visualization and Quantitation of Multiple Steroid Hormones Based on Signal-Amplified Biosensing with Duplex Molecular Recognition. *Chem. Eur. J.* **2017**, *23*, 10683−10689.
(42) Li, Q.; Wang, Z.; Chen, Y.; Zhang, G. Elemental Bio-Imaging of PEGylated $NaYF_4$:Yb/Tm/Gd Upconversion Nanoparticles in Mice by Laser Ablation Inductively Coupled Plasma Mass Spectrometry to Study Toxic Side Effects on the Spleen. *Liver and Kidneys. Metallomics* **2017**, *9*, 1150−1156.
(43) Li, X.; Zhu, J.; Man, Z.; Ao, Y.; Chen, H. Investigation on the Structure and Upconversion Fluorescence of Yb^{3+}/Ho^{3+} Co-doped Fluorapatite Crystals for Potential Biomedical Applications. *Sci. Rep.* **2015**, *4*, 4446.
(44) Chen, W.; Zhang, Y.; Yeo, W. S.; Bae, T.; Ji, Q. Rapid and Efficient Genome Editing in *Staphylococcus aureus* by Using an Engineered CRISPR/Cas9 System. *J. Am. Chem. Soc.* **2017**, *139*, 3790−3795.
(45) Xiu, W. J.; Shan, J. Y.; Yang, K. L.; Xiao, H.; Yuwen, L. H.; Wang, L. H. Recent Development of Nanomedicine for the Treatment of Bacterial Biofilm Infections. *View* **2021**, *2*, 20200065.

https://doi.org/10.1021/acsnano.1c11333
ACS Nano 2022, 16, 3300−3310